Combined photoacoustic and photoconductive spectroscopic investigation of nonradiative recombination and electronic transport phenomena in crystalline *n*-type CdS. I. Experiment

Andreas Mandelis and Edwin K. M. Siu
Photoacoustic and Photothermal Sciences Laboratory, Department of Mechanical Engineering, University of Toronto, Toronto, Ontario, Canada M5S 1A4
(Received 1 April 1986)

Microphone gas-coupled photoacoustic spectroscopy (PAS) and photocurrent spectroscopy (PCS) have been applied simultaneously to high-resistivity, (0001)-oriented, single crystals of pure *n*-type CdS in order to obtain detailed information about the importance of the nonradiative capture or recombination channels at defect states below the band-gap energy of these materials. The primary spectral responses of well-characterized samples at open circuit and in the presence of perturbing transverse ac or dc electric fields, as well as secondary PA and PC spectra were found to be largely consistent with a substantial enhancement of the nonradiative recombination quantum efficiency at sub-band-gap wavelengths, concomitant with free-carrier trapping at defect centers (presumably sulphur vacancies) responsible for the observed red quenching of the photoconductivity. Our combined spectroscopic approach, besides the new direct information it yields concerning intrinsic band-to-band transition contributions to the PA and PC spectra as well as band-gap defect structure information, is also shown to raise the level of confidence regarding data interpretation through consistency arguments between the PAS and PCS results, an insight not easily obtained solely through conventional PC or optical-absorption measurements.

I. INTRODUCTION

Over the past few decades a number of studies have been performed on the optical[1–3] and the photoconductive[4–6] properties of single-crystalline CdS at room temperature. The application of photoacoustic and photothermal spectroscopic techniques to the characterization of electronic properties and defect structures of this and other II-VI compound semiconductors is of importance because of the unique ability of these techniques to yield *direct* information about nonradiative deexcitation energy channels operating in optically excited materials. The presence of native defects, specifically sulphur vacancies and cadmium interstitials,[6] in pure CdS crystals has been shown to be responsible for several peaks in the photoconductivity spectrum near the band edge of this material. The intensity and spectral position of these peaks is strongly related to the preparation history of the sample used for a given experiment[6] and its impurity content.[7] These, and conceivably other, factors have amounted to notable differences in the reported spectral responses of different crystalline CdS samples with respect to the appearance of sub-band-gap features.[6,8,9] The use of photoacoustic spectroscopy,[9] with the polarization of the exciting radiation perpendicular or parallel to the crystal *c* axis has helped distinguish between nonradiative peaks P_1 (509 nm), P_3 (518 nm), and P_6 (544 nm) and peaks P_2, P_4, P_5, and P_7 due to luminescent states, since the latter peaks were absent from the photoacoustic spectrum. Recently, Bandeira *et al.*[10] performed a study of the dependence of the photoacoustic signal on the magnitude of an applied dc electric field across a CdS crystal of unknown origin and specifications. These authors produced experimental and electron transport-related theoretical results, taking into account carrier diffusion and recombination. Their theory showed the same general spectral trends as the experiments under the assumptions of (i) negligible trapping state densities and (ii) constant nonradiative quantum efficiencies throughout the spectral region of interest (460–580 nm). The electronic and photoconductive behavior of CdS is, however, intimately related to the defect morphology of this material.[4,6] Very recent experimental evidence on this semiconductor shows that the photoacoustic spectral response is also a sensitive function of impurity content,[11] surface preparation[12] and native defect concentrations,[9,13] especially in the sub-band-gap region. Furthermore, the existence of nonradiative peaks at the low-energy side of the *A*-, *B*-, and *C*-exciton absorption bands in CdS at room temperature is strongly indicative of a spectrally variable, wavelength-dependent nonradiative quantum yield. In this work, an experimental program was undertaken to elucidate the role of (i) sub-band-gap defect states and (ii) intrinsic band-to-band electron-hole recombination in shaping the photoacoustic (PA) and photoconductive (PC) spectral responses of well-characterized high-resistivity pure *n*-type CdS crystals. The experimental evidence presented herein may be considered a detailed generalization of, and an extension to, the work by Bandeira *et al.*[10] in sub-band-gap spectral regions where defect densities are important and the wavelength dependence of the nonradiative quantum efficiency may be significant.

II. MATERIALS AND EXPERIMENTAL PROCEDURE

Samples used in this work were high-purity CdS single crystals $10\times5\times1.5$ mm^3 in size and nominal resistivity $\rho=1\times10^6$ Ω cm, from Eagle-Pitcher, Inc. (Miami, Oklahoma). Crystal growth of the cadmium sulphide crystals was carried out by the chemical vapor transport method[14] in the following manner,[15] which is essentially a variation of the technique described by Cutter and Woods:[16] Powders of the elemental components of the compound were exposed to higher than stoichiometric partial pressure of sulphur vapor and further sintered (densified) into a chunk of compound material. The resulting compound was then vaporized at 1260 °(C) for 190 hours, then it was cooled down to 1210 °(C), at which temperature the sublimed compound was grown to a crystal boule with nonstoichiometric excess of S^{2-} ions[6]. Crystals grown in this manner have been found[17] to contain large densities of native defects such as vacancies and interstitials of both elemental components and they exhibit a natural *n*-type character to an extent determined by the degree of self-compensation and the defect density in the crystal.

A CdS crystal from the above batch, cut with the *c* axis perpendicular to the surface (0001) plane, was first etched for 20 s in 95% by volume of 3*M* HCl and 5% by volume of 30% H_2O_2 in water to remove any surface damage which might distort the PA spectrum at and below the band-gap energy.[12] The crystal was further contacted along the narrow 5×1.5 mm^2 opposite surfaces with a mixture of Ga and In amalgam in semiliquid form. It has been established[18,19] that Ga and In form good Ohmic contacts with CdS, due to a small potential barrier height at the interface, i.e., $\phi_1-\chi_2\leq0.1$ eV, where ϕ_1 is the metal work function and χ_2 is the electron affinity of the semiconductor. The crystal-amalgam system was placed in a nitrogen flow oven at 350 °C for 2 h to allow the metal mixture to diffuse in the semiconductor bulk in order to reduce the contact resistance. After the thermal cycle, the crystal was cooled inside the oven to 100 °C and pulled out. Ohmicity was checked using a 22-Ω resistor and a dc voltage supply connected in series with the crystal. The photocurrent was measured at various voltages by illuminating the crystal with a constant radiance light source. Figure 1 shows the current-voltage characteristics of the crystal, which exhibits Ohmic behavior for both signs of the applied electric field. The slight change in the slope upon reversal of the field is not fully understood and may be due to local changes in the field magnitude because of defect and impurity generated inhomogeneities in the illuminated region.[20]

The experimental configuration for PA and PC spectroscopic investigation is shown in Fig. 2. The light source for primary PA and PC spectra was a 1000 W xenon lamp (Oriel Corp. model 8540) with output wavelength ranges from approximately 270 to 900 nm. The emerging light was monochromatized (Instruments SA Inc. monochromator model H-20) and focused onto the sample chamber of a photoacoustic cell (EG&G model 6003) with the sample holder redesigned to accommodate the electrical circuitry. The PA signal was preamplified (EG&G model 6005) and lock-in analyzed (EG&G model 5204). The PC response was measured via the voltage drop across a 1.5 Ω series resistor and this signal was also preamplified (Keithley model 427) and lock-in analyzed. Under our experimental conditions, the resistance of the CdS crystal was about 4 kΩ, therefore the external series resistor represented a negligible perturbation to the optoelectronic characteristics of the circuit.

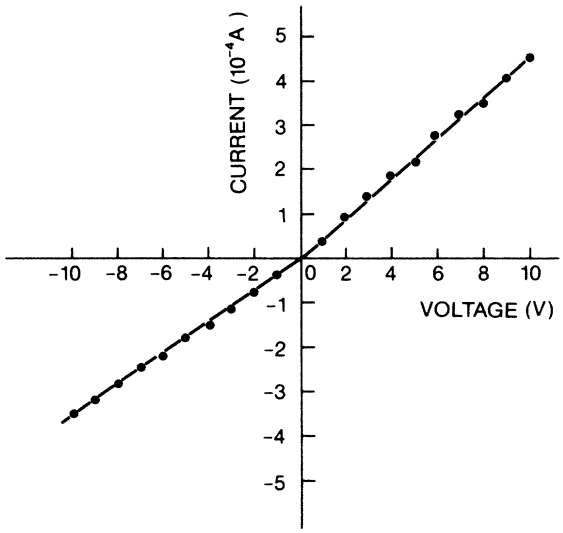

FIG. 1. Current-voltage characteristics of *n*-type CdS high purity single crystal.

Four basic categories of experiments were performed on the same CdS crystal: The first set of experiments involved PA absorption and transmission measurements. For the PA absorption spectrum, the $10\times5\times1.5$ mm^3 sample was placed inside the modified holder in the open-circuit configuration. For the PA transmission spectrum, a larger crystal from the same batch was placed outside the PA cell, on top of the quartz window. Transmitted radiation was detected by a black body inside the cell. This technique has been shown[21] to generate transmission spectra of semiconductors, which are very similar to transmission spectra obtained by other conventional methods. Furthermore, it has the advantage of a *direct* comparison between the PA and the transmission spectrum of the sample, since they were both obtained using the same equipment and the same lamp throughout normalization spectrum.

The second set of experiments involved primary PA and PC spectroscopic measurements using chopped (modulated) irradiation with an applied transverse dc electric field across the crystal inside the photoacoustic cell. The laboratory was kept in nearly complete darkness during these experiments to eliminate the influence of background radiation on the photosensitive sample.

The third set of measurements was performed with optical excitation using unmodulated (dc) light and an applied transverse ac electric field, under the same experimental conditions used for the previous set of measurements.

The fourth experimental set was performed to obtain

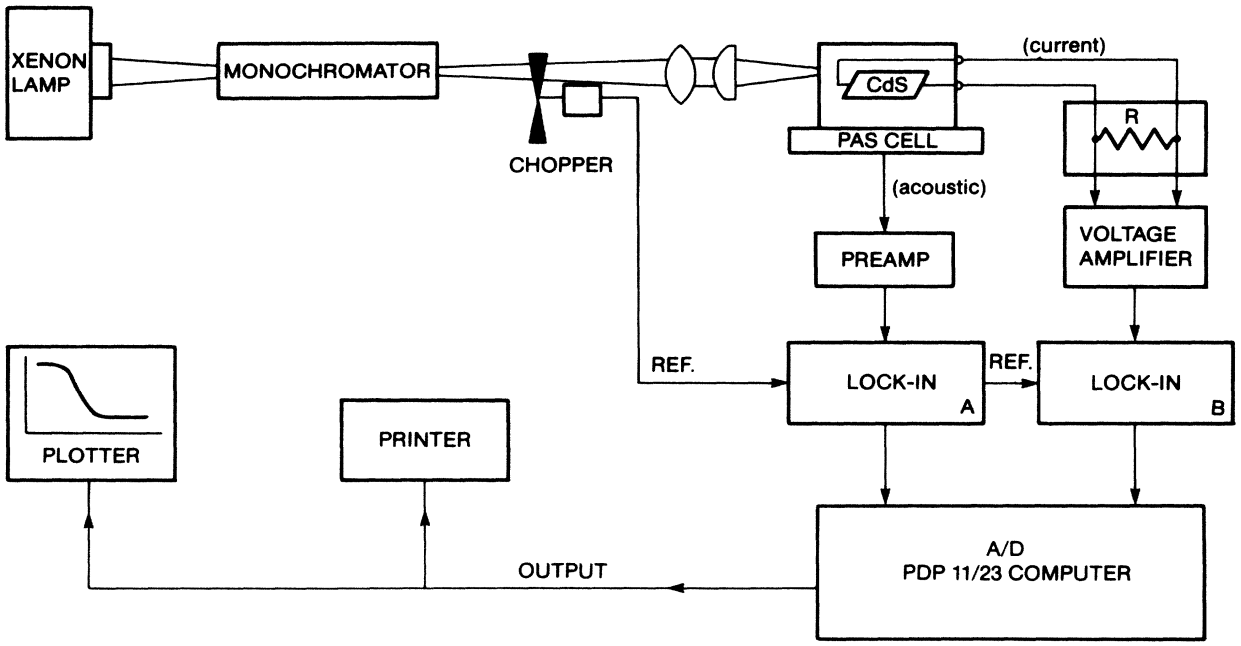

FIG. 2. Schematic diagram of the experimental apparatus for PA and PC measurements.

secondary PA and PC spectra in order to study the effect of the occupation of defect (trap) centers on the CdS response. The primary light source was an unmodulated broadband table lamp. As the secondary source, the modulated light from the Xe arc lamp was monochromatized and allowed to irradiate the sample in the presence of a transverse dc electric field.

III. EXPERIMENTAL RESULTS AND DISCUSSION

A. PA absorption and transmission spectra

The magnitude and phase of the PA absorption spectrum of CdS are shown in Fig. 3. On the high-energy side of the spectrum, the PA response exhibits a plateau below approximately 500 nm, followed by a monotonic decrease toward a minimum at approximately 530 nm. It then rises slightly and essentially levels off at approximately 555 nm. Earlier work on CdS PA magnitude spectra obtained by microphone gas-coupled photoacoustic apparatus, sometimes does show similar sub-band-gap signal contributions with CdS in powdered form[22] and in single crystalline form.[23] Yet, spectra obtained by other workers show little or no evidence of sub-band-gap features, either in the powdered[24] or single crystalline[10] form. Comparisons between these seemingly conflicting pieces of experimental evidence are, however, difficult to make as in most reports no information is given as to the origins and characterization of the samples used. Another complication is that PA spectra obtained by reverse-side detection in a microphone gas-coupled system,[25] or with piezoelectric transducers attached to the back of a CdS sample illuminated from the front,[9,13,26] have exhibited great differences from those obtained using front-side illumination and detection by a microphone,[10,23] and from those obtained piezoelectrically with the sample illuminated from the back.[13,26] Hata *et al.*[26] have concluded that the former class of experiments yields PA information corresponding to the exciton levels and nonradiative electronic states in CdS, whereas the latter class of experiments (to which the present work belongs) gives PA spectra corresponding to the fundamental absorption characteristics of the material.

Our PA phase, Fig. 3(b), appears flat over the super-band-gap region, followed by a monotonic increase in the *lag* with a maximum at about 525 nm. The phase lag subsequently decreases to about 555 nm and exhibits saturation at longer wavelengths at a level higher than the super-band-gap phase. A similar spectral behavior of the phase of a CdS single crystal in a microphone gas-coupled PA cell has been observed by Takaue *et al.*,[25] albeit with a broader lag maximum around 540 nm. The PA magnitude corresponding to the conventional phase data using front-side irradiation was reported in Ref. 25 and exhibits monotonically decreasing sub-band-gap contributions with no evidence of a local minimum, unlike that shown in Fig. 3(a).

One of the early applications of PAS to semiconductors was the determination of the energy gap width from the PA spectral response. Breuer[27] has estimated the band-gap energy of a CdS single crystal to be 2.4 eV, based on the location of the "knee" formed by the absorption edge of the spectrum. CdS band-gap width values have been obtained using various techniques[1,28–30] and range between 2.39 and 2.53 eV at room temperature. Recently, Rochon and Racey[21] discussed the error committed on the determination of the band-gap width from PA spectra, due to the onset of photoacoustic saturation at the strong absorption side of the band-gap region of semiconductors.

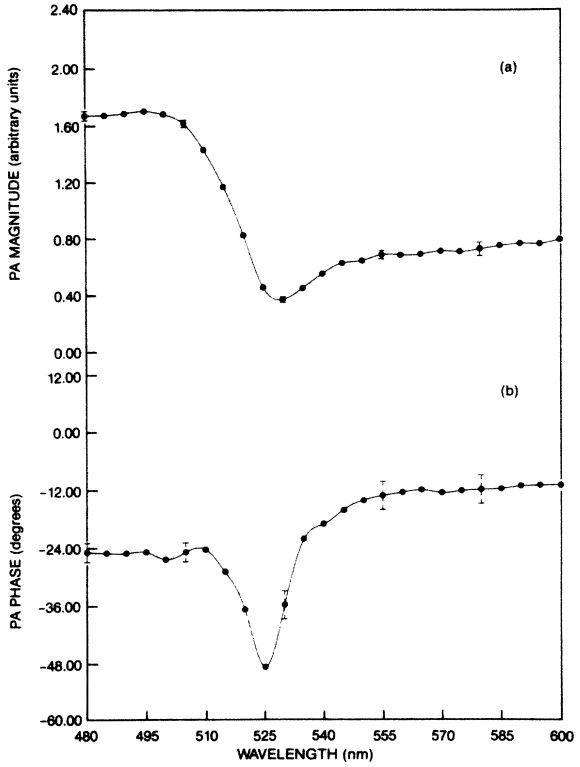

FIG. 3. PA absorption spectrum of CdS. Modulation frequency, 50 Hz; spectral resolution, 2 nm. (a) Magnitude; (b) phase.

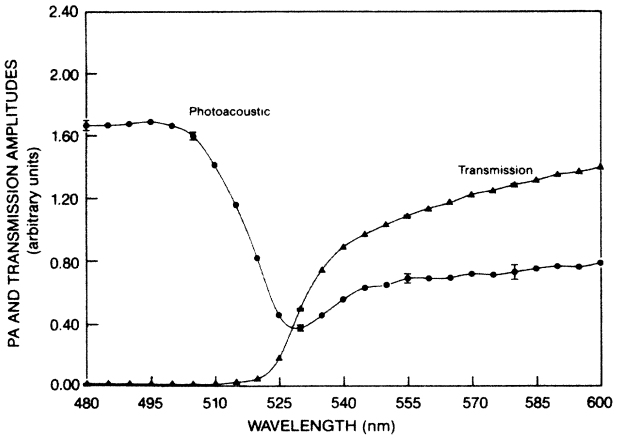

FIG. 4. Magnitudes of (a) PA absorption and (b) PA transmission spectrum of n-type CdS. Modulation frequency: 50 Hz; spectral resolution: 2 nm.

These authors thus concluded that the break in the curve of the PA absorption spectrum of GaSe at approximately 2 eV cannot be used to determine its band-gap energy. Based on similar reasoning, it can be argued that the band-gap energy of our CdS crystal may be somewhat larger than the 2.45 eV, which the knee of the PA magnitude spectrum indicates in Fig. 3(a). Figure 4 shows the CdS PA transmission spectrum together with the PA absorption spectrum from Fig. 3(a). In the absence of polarization of the incident optical field, no exciton formation is apparent in the transmission spectrum in the 485—500 nm region.[2,6] Uchida[6] determined photoconductively the spectral positions of the A, B, and C excitons at room temperature (501.5, 498, and 485.5 nm, respectively) due to the presence of three twofold degenerate valence bands in CdS, the highest band having Γ_9 symmetry and the remaining two having Γ_7 symmetry.[31] The lowest-energy excitons have been shown[3] to have ionization energies of about 0.028 eV. Based on the small ionization energies, Smith[32] has shown that it was possible to assign exciton energy levels similar to shallow donor states very close to the conduction band. Exciton formation in CdS is thus expected to occur at photon energies slightly lower than the band-gap energy. Since the highest-energy C-exciton series have formation energy around[6] 2.55 eV, we estimated the value $E_g \approx 2.56$ eV as a more accurate representation of the band-gap energy than the 2.45 eV obtained from the PA absorption spectrum knee.

Toward the long-wavelength region in Fig. 4, the PA transmission spectrum does not exhibit the expected anticorrelation with the PA absorption spectrum. A possible reason for this discrepancy is a spectral variation of the fraction of the absorbed energy which is converted into heat through nonradiative deexcitation. In our CdS crystal we have visually observed the occurrence of orange luminescence at room temperature, in agreement with photoluminescence (PL) data obtained[11] from undoped n-type CdS low-resistivity single crystals. Careful observation of the wavelength dependence of PL in our sample revealed that the orange luminescence ceased at wavelengths longer than around 525 nm. This limit corresponds closely to the rise of the PA absorption response curve for $\lambda > 530$ nm in Figs. 3 and 4. It can therefore be concluded, at least qualitatively, that for our pure n-type CdS single crystal, a likely explanation for the observed PA absorption and transmission spectra (Fig. 4) is the wavelength dependence of the radiative and nonradiative quantum yields, with a more efficient conversion of the optical to thermal energy for $\lambda \geq 530$ nm corresponding to the virtual shut-off of the PL channel as shown in the work by Wada *et al.*[11] A theoretical model supporting the above assertion is presented in Paper II of this work. In further support of this argument, it has been shown experimentally by Lambe[33] that the broad, red photoluminescence observed at room temperature in undoped CdS decays much faster than the photocurrent response during the half cycle of darkness following an impulse of UV (3650 A) excitation. This result implies that the radiative quantum efficiency is greater than the nonradiative quantum efficiency in the spectral region of interest,

$$\eta_{\text{rad}} = \tau/\tau_{\text{rad}} > \eta_{\text{nonrad}} = \tau/\tau_{\text{nonrad}} , \tag{1}$$

where τ is the total (observed) excited state lifetime, τ_{rad} is the radiative lifetime, and τ_{nonrad} is responsible for the photocurrent decay via electron-hole recombination and heat generation. Lambe assumed recombination between an electron trapped in a donor level about 1.5 eV above the valence band and a free hole. These considerations indicate that when both radiative and nonradiative recombination pathways are allowed in a pure CdS single crystal at room temperature, the radiative recombination rate

predominates over the nonradiative rate. This is consistent with theoretical results on the relative magnitudes of these rates in direct-gap semiconductors[34] and would explain the PA absorption minimum at about 530 nm in Fig. 4, as well as the increase in the nonradiative quantum yield for $\lambda > 530$ nm in terms of a reversal of the relative magnitudes,

$$(\tau_{\text{nonrad}})^{-1} > (\tau_{rad})^{-1}; \quad \lambda \geq 530 \text{ nm} .$$

The phase lag of the PA absorption spectrum in Fig. 3(b) is mainly dominated by two time-delayed processes, i.e., the time decay between light absorption and heat generation and that between heat generation and pressure rise in the PA cell.[35] The former process is governed by the excited state lifetime[35,36] of the crystal, and the latter by the thermal diffusion time to the surface.[35] In the short-wavelength side of the Fig. 3(b) ($\lambda < 500$ nm) the optical energy is deposited very close to the crystal surface due to strong intrinsic absorption. The time delay between heat generation and PA signal production is, therefore, expected to be independent of the absorption characteristics of the crystal[35] (photoacoustic saturation) and is probably dominated by the excited state (electron-hole band-to-band) recombination lifetime.[36] The flat character of the phase lag at super-band-gap wavelengths is thus indicative of essentially constant nonradiative lifetime τ_{nonrad} and therefore constant quantum efficiency η_{nonrad} in that region. Between 500 and 525 nm, the optical-absorption coefficient decreases (Fig. 4, transmission curve), and the thermal energy centroid moves from the surface to the bulk of the crystal, as thermal diffusion dominates the increasing phase lag. The sharp reduction of the phase lag for $\lambda \geq 525$ nm, combined with the cessation of visible orange luminescence and with the monotonic decrease in the optical-absorption coefficient [Fig. 3(b)], is consistent with the domination of the PA phase by a rapidly decreasing τ_{nonrad} with a concomitant increase of η_{nonrad} in this spectral region.[36]

B. Primary PA and PC spectra: modulated optical excitation with a dc electric field

Figure 5 shows the amplitudes and phases of the PA and PC spectra of CdS under illumination modulated at 20 Hz and an applied transverse dc electric field of 10 V. The amplitudes of both PA and PC responses are low at super-band-gap energies. They rise at lower energies, with the PA signal exhibiting a local maximum at around 517 nm, while the PC signal shows evidence of a broad shoulder around the same spectral region. Both spectra exhibit maxima at about 529 nm and decrease monotonically at longer wavelengths. Both phase spectra, Fig. 5(b), show phase-lag increases with increasing wavelength and they both level off at $\lambda \geq 530$ nm.

The occurrence of the two PA amplitude peaks was not observed experimentally by Bandeira *et al.*,[10] presumably due to the poor spectral resolution of their experiment ($\Delta\lambda \approx 10$ nm). Uchida[6] has also studied the photoconductive responses of several pure CdS crystals heat-treated in different partial pressures of sulphur vapor. Those crystals were obtained from the same manufacturer as ours

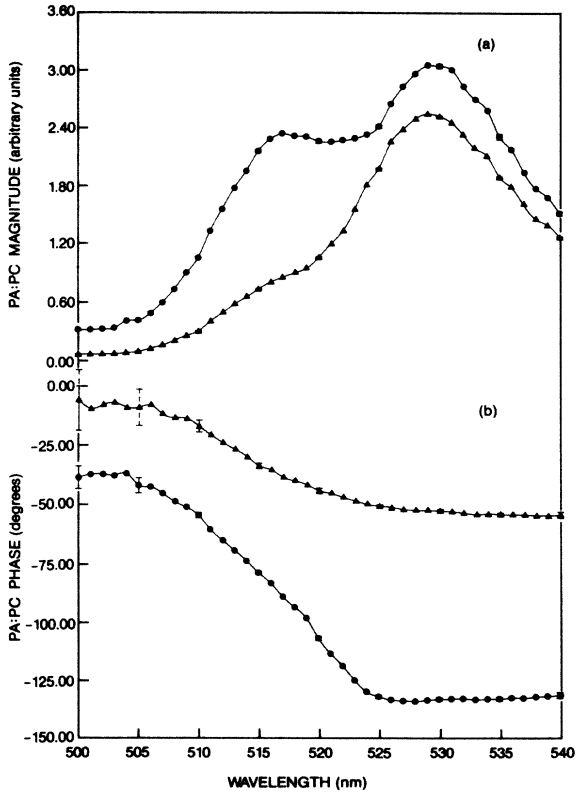

FIG. 5. (a) Magnitude spectra of PA (—●—●—), and PC (—▲—▲—) responses with a transverse electric field of 10 V dc. Light modulation frequency: 20 Hz; spectral resolution: 2 nm. (b) Phase spectra of PA (—●—●—), and PC (—▲—▲—) responses.

and, when used by Uchida for PC studies, had a growth and thermal cycle history similar in many ways to our crystals. A particular crystal was heat-treated in $p_s = 20$ mm Hg for 1 h at 850 °C and exhibited a dramatic increase in resistivity, such that $\rho \geq 10^6$ Ω cm. The PC spectral response of that crystal under an applied voltage of 6 V dc showed (Fig. 2, Ref. 6) a broad band with a maximum located at 532 nm in good agreement with the spectral features of Fig. 5(a). The position of that peak, identified by Uchida as P_5, was associated with the photoexcitation of a valence-band electron to a doubly ionized donor defect state identified as a sulphur vacancy V_s^{2+}, followed by thermal release from this level to the conduction band as shown in Fig. 6. Wasa *et al.*[9] showed the luminescent nature of the spectral peak P_5 through its absence (a "trough") from the piezoelectrically detected CdS PA spectrum illuminated from the front side at 534 nm and after comparison with the PL spectrum of that material, in which P_5 appeared as a peak of 531 nm. These authors used the same comparison between PL and PA spectra to establish the nonradiative nature of Uchida's PC peak P_3 (517 nm). The PA spectral position of P_3 was thus found[9] to be 518 nm. The nonradiative nature of P_3 was later confirmed photoacoustically by Hata *et al.*,[13] who placed its spectral position at 519 nm. In

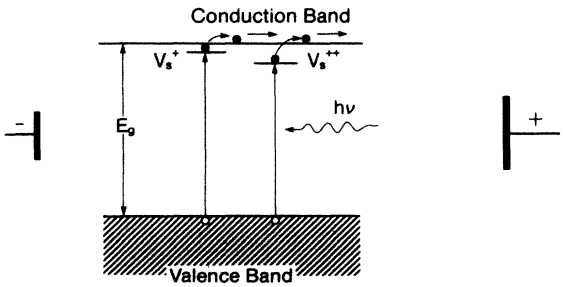

FIG. 6. Energy diagram of the proposed (Ref. 6) transition mechanism for photo-excited electrons to native defect sulphur vacancy donor states. V_s^{2+}: doubly ionized defect responsible for spectral peak P_5 (532 nm); V_s^+: singly ionized defect responsible for peak P_3 (517 nm) observed in some sulphur vapor treated CdS crystals.

view of the nonradiative nature of the P_3 peak, it might appear reasonable to associate the PA maximum at 517 nm in Fig. 5(a) with this peak. The luminescent nature of P_5, in Uchida's work would not, however, be compatible with the PA maximum at 529 nm in Fig. 5(a). Bandeira *et al.*[10] observed only one PA peak at around 523 nm with their uncharacterized CdS crystal, which they attributed to carrier diffusion within the crystal due to band-to-band excitation under conditions maximizing the PA signal. From their electron transport-related theoretical model of the PA signal generation in the semiconductor, they found that the maximum in the PA response occurred at a wavelength λ_{max}, such that the CdS absorption coefficient β was approximately equal to the inverse of the electron diffusion length L,

$$\beta(\lambda_{max}) \approx [1/L(\lambda_{max})][1+(\omega\tau_{BB})]^{1/4} , \quad (2)$$

where ω is the angular light modulation frequency and τ_{BB} is the electron lifetime in the conduction band. In the framework of that model the PA response maximum is expected to shift to higher energies (higher β) with increased modulation frequency.

This was easily observed with theoretical curves (Fig. 8, Ref. 10) and was also supported by our own experimental results, but was not conclusively supported by the experiment of Bandeira *et al.* (Fig. 6, Ref. 10), perhaps due to the poor spectral resolution of that work. Bube[37,38] has done extensive work on the PC spectral response of pure CdS crystals and observed photocurrent maxima between 515 and 520 nm. These maxima were assigned to the intrinsic excitation transition from the valence to the conduction band, as they correspond closely to the CdS absorption edge. This interpretation is essentially in agreement with the basic assumptions of the model by Bandeira *et al.*,[10] which is, however, expected to break down at sub-band-gap spectral regions, as it neglects all contributions to the PA signal from impurity states within the bandgap and any spectral dependence of the nonradiative quantum yield.

Based on the above considerations, we attributed the high-energy PA peak in Fig. 5(a) and the PC shoulder in Fig. 5(b) to the intrinsic excitation. The peak wavelength at 517 nm is within the range of peak responses established by Bube.[37,38] It is unlikely that this peak is excitonic in nature, since excitons are not likely to exist in pure CdS crystals at room temperature.[39] Uchida[6] has reported, however, that excitonic peaks appear at room temperature in the PC spectrum of CdS crystals with very high sulphur content, with the lowest-energy exciton A located at 501.5 nm, well above the 517-nm maximum observed in Fig. 5(a). Wasa *et al.*[9] confirmed Uchida's observation by studying PA spectra produced with light polarized parallel and perpendicular to the c axis of an uncharacterized CdS crystal. They observed the A excitonic peak to disappear in the $\mathbf{E}||c$ field configuration, in agreement with the quantum-mechanical selection rule governing the interband transition from the A-valence band to the conduction band,[40] and thus they placed exciton A at 506 nm. The cause of the pronounced difference between the PA and PC responses around 517 nm in Fig. 5(a), as expressed in terms of the fully resolved PA peak versus an unresolved PC shoulder must be sought in the different nature of the two types of spectroscopic measurements: The PA technique probes a thickness in the material on the order of the thermal diffusion length,[41]

$$\mu_s(f) = (\alpha_s/\pi f)^{1/2} , \quad (3)$$

where α_s is the thermal diffusivity of the material. Using[42] $\alpha_{CdS} = 0.15$ cm^2/s and $f = 100$ Hz, we find μ_s (100 Hz) ≈ 22 μm. The PC technique is sensitive to carrier transport through distances on the order of the electron diffusion length (about 1 μm), which causes different depths of the sample to be probed by the two methods. The larger PA phase lag, Fig. 5(b), is also consistent with probing a larger depth than the PC phase spectrum. A similar argument has been advanced to account for differences in spectral features obtained through probing semiconductors with a combination of PC and photothermal deflection (PD) spectroscopies.[43]

In the spirit of the discussion in subsection A of this section, we attributed the rise in the PA spectrum at $\lambda \geq 522$ nm in Fig. 5(a) to the spectral dependence of the nonradiative quantum efficiency of the deexcitation process, and specifically to a substantial increase in $\eta_{nonrad}(\lambda)$ in the $\lambda \geq 522$ nm region. This interpretation is consistent with the results shown in Figs. 3 and 4 under open-circuit conditions and with the theoretical model presented in Paper II of this work. It would further lead to the complete dependence of both PA and PC peaks at 529 nm on the fractional increase in η_{nonrad}, as shown in Paper II.

Several experiments were further performed with the magnitude of the applied transverse dc voltage varying between 0 and 30 V. The PA spectral magnitude and phase responses are shown in Figs. 7(a) and 7(b), respectively. The phase lags show a consistent increase with increasing electric field magnitude. This can be explained from the consideration that Joule heating most probably dominates[10] the heat generation processes at high V_a (≈ 30 V). The Joule heating effect is a phenomenon primarily associated with electric fields in the bulk of the semiconductor, and consequently the phase lag is expected to be large and spectrally constant. At lower values of V_a, heat contributions due to nonradiative recombination events are expected to become comparable to, and eventually dom-

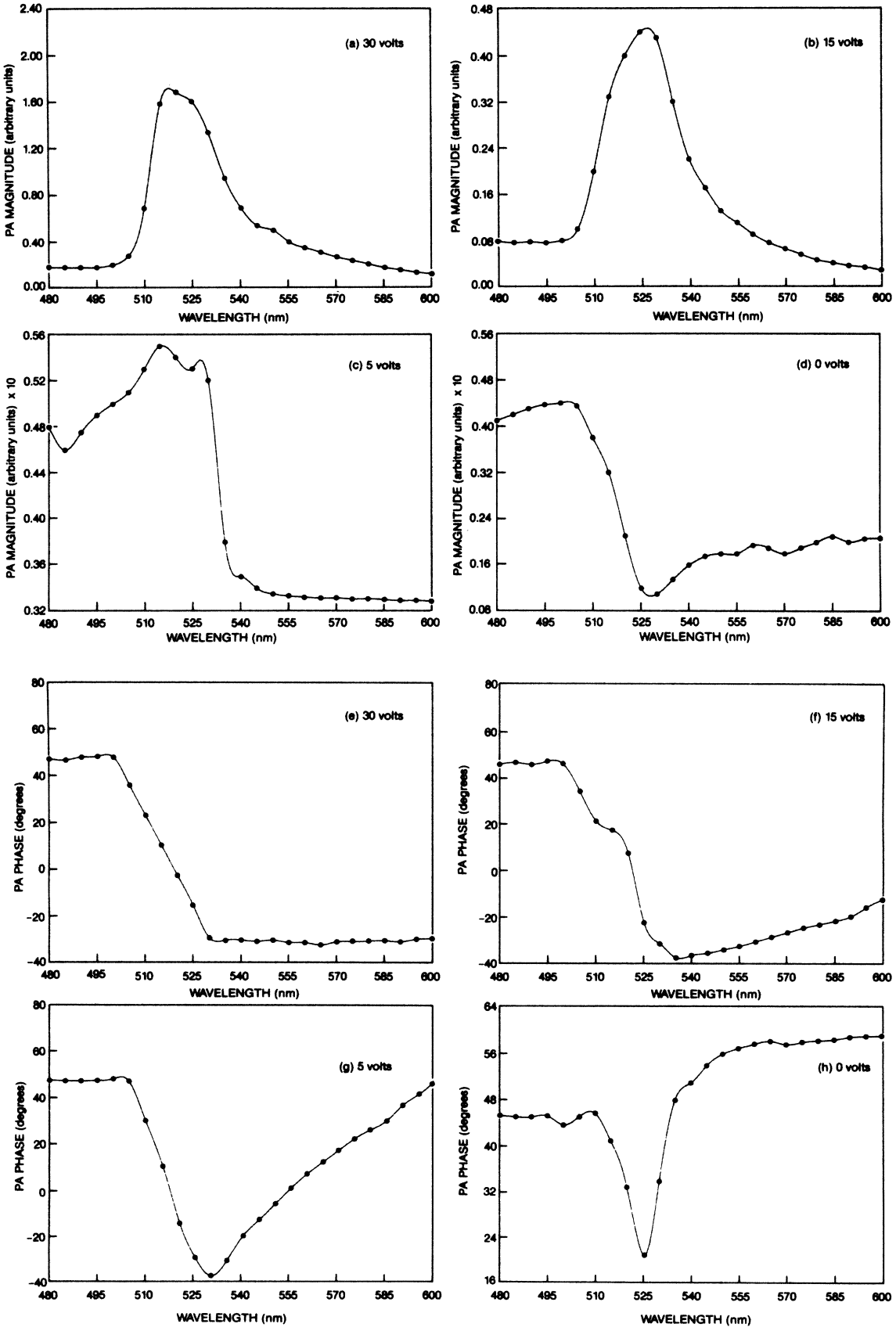

FIG. 7. PA spectral responses of CdS under an external dc transverse electric field: (a),(e) 30 V; (b),(f) 15 V; (c),(g) 5 V; (d),(h) 0 V. Light modulation frequency: 20 Hz; spectral resolution: 2 nm (a)—(d) PA magnitudes; (e)—(h) PA phases.

inate, the Joule effect. Nonradiative recombination is mostly a surface-related process, especially in the presence of a finite surface state density, and thus a gradual move of the heat centroid from the bulk toward the surface is expected with decreasing V_a, resulting in smaller PA phase lags in agreement with the trends shown in Figs. 7(e)–7(h). The PA magnitude data of Figs. 7(a)–7(d) display a strong enhancement of the sub-band-gap signal with decreasing V_a, which dramatically increases the average sub-band gap-to-peak signal ratio. This ratio is approximately 12 in Fig. 7(a) and 1.6 in Fig. 7(d). The trend is consistent with a receding long-wavelength thermal source from the surface into the bulk of the crystal with increasing V_a, resulting in a decreased relative importance of the sub-band-gap contribution to the PA signal. The trend of increasing absolute peak PA magnitude with increasing V_a has previously been observed by Bandeira *et al.*[10]

The PA and PC spectra under an applied dc field $V_a=20$ V were further investigated with the light modulation frequency as a parameter varying between 20 and 200 Hz. The experimental results are shown in Fig. 8. From the PA spectra of Fig. 8(a) it was observed that the ratio of the 517-nm-magnitude peak to the 529-nm peak increases with increasing modulation frequency. Up to 4-nm peak shifts to higher photon energies with increasing frequency are observed, such as were predicted by the theory presented by Bandeira *et al.*[10] These blue shifts tend to confirm the intraband excitation nature of the PA peak located at 517 nm at 20 Hz. No measurable spectral shift of the 529 nm PA and PC peaks was observed in Figs. 8(a) and 8(b). Figure 9 shows plots of the frequency dependence of the 517 and 529-nm PA magnitude peak signals. According to the Rosencwaig and Gersho (RG) theory[41] a f^{-1} dependence is expected in the spectral region where the sample is optically opaque, such as the 517-nm peak, and thermally thick; further, a $f^{-1.5}$ dependence is expected in the region where the sample is optically transparent, such as the 529-nm peak, and thermally thick. In both peak wavelengths $(\mu_s)_{\max}=\mu_s(20\text{ Hz})=49$ μm, i.e., our 1.5-mm-thick sample was thermally thick. Using $\beta(517\text{ nm})=(150\text{ cm}^{-1})^2$ and $\beta(529\text{ nm})=(4\text{ cm}^{-1})^3$, it was concluded that both peak signals satisfied the μ_s versus β^{-1} relationship criteria of the RG theoretical case limits[41] 1c (529-nm peak) and 2b (517-nm peak). There is an additional f^{-1} contribution to the PA signal from our sample due to the Joule effect in the presence of the external dc electric field.[10] Therefore, the overall theoretical frequency dependence to be compared with Fig. 9 is f^{-2} for the 517-nm peak and $f^{-2.5}$ for the 529-nm peak. The observed dependences are $f^{-1.8\pm0.1}$ and $f^{-2.3\pm0.1}$, respectively, and are in good agreement with the theoretical predictions. The relative difference in frequency dependence (i.e., in slopes S) between the two curves of Fig. 9 is $S_{530\text{ nm}}-S_{517\text{ nm}}=0.5$, and its indicative of our PA signal compliance with the RG theory. The same difference has been reported[13] between the

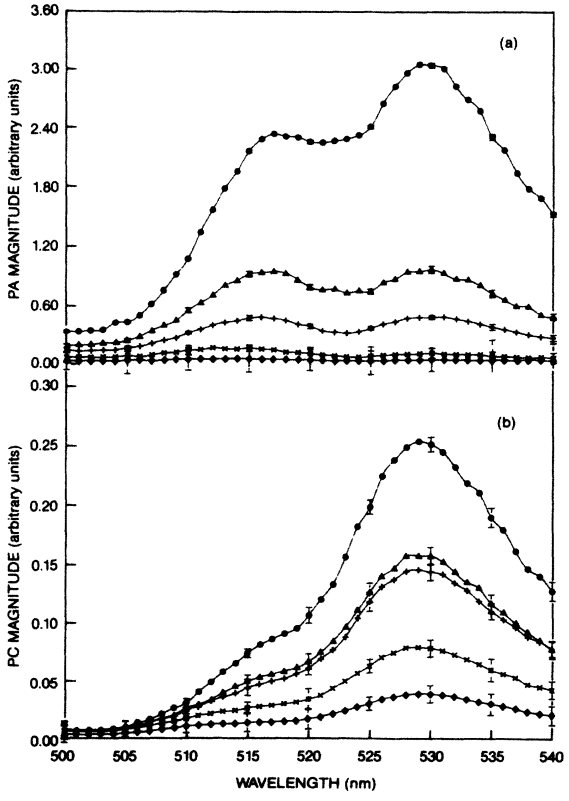

FIG. 8. (a) PA and (b) PC magnitude spectra of CdS with a 10 V dc applied electric field and 2-nm spectral resolution. Light modulation frequency: 20 Hz (—●—●—); 35 Hz (—▲—▲—); 50 Hz (—+—+—); 100 Hz (—x—x—); and 200 Hz (—◆—).

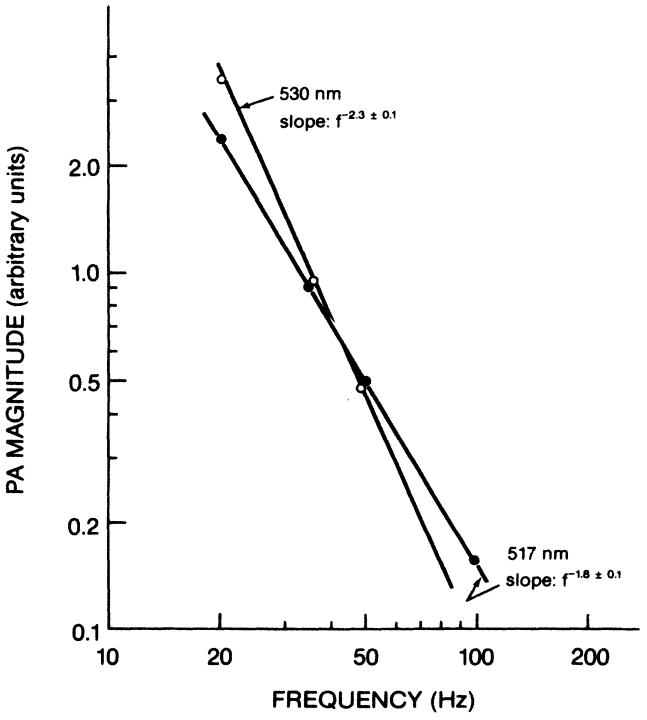

FIG. 9. CdS PA magnitude frequency dependence: (—○—○—), 529 nm peak; (—●—●—), 517 nm peak.

slopes of PA magnitude versus frequency curves for a CdS single crystal irradiated in the optically opaque (420 and 450 nm) and the transparent (632.8 nm) spectral regions. The absolute powers of the frequency dependencies, however, were different in that work, as it was performed under open-circuit conditions and with a $LiNbO_3$ transducer with different PA frequency response characteristics from those of the microphone gas-coupled system.

C. Primary PA and PC spectra: Unmodulated optical excitation with an ac electric field

There is a major difference between this mode of experimentation and the preceding one. In this mode, *only* the thermal energy due to the Joule effect contributes to the photoacoustic and modulated PC signals. This is so because thermal energy from nonradiative carrier recombination is not temporally modulated and thus will not be detected by the PA and PC probes. Therefore, a simple interpretation of the experimental responses, consistent with the data of Subsection B is expected with this mode of experimentation.

The magnitudes and phases of the PA and PC spectra with a 20-V peak-to-peak AC electric field applied across the CdS crystal are shown in Fig. 10. The PA magnitude in Fig. 10(a) exhibits a maximum and an unresolved shoulder. A comparison with the PA magnitude of Fig. 5(a) shows that the long-wavelength maxima are located at 529—530 nm, i.e., in the same spectral location, while the peak position of the shoulder in Fig. 10(a) is located at $\lambda \geq 523$ nm, a shift of ≈ 6 nm from the secondary peak at 517 nm in Fig. 5(a). The PC magnitudes, however, exhibit similar spectral features under both chopped and unmodulated illumination. Fig. 10(b) shows an increase in the lag of the PA phase spectrum at sub-band-gap wavelengths, while the PC phase is spectrally flat. The presence of the PA shoulder at about 523 nm may be tentatively associated with the spectral shift of the peak at 517 nm in Fig. 5(a) attributed to the band-to-band electronic transition. According to Eq. (2), there will be a red spectral shift of the PA maximum due to interband excitation with decreasing optical modulation frequency. The spectrum of Fig. 10(a) can be thought of as the limiting case with $\omega \rightarrow 0$; in this limit the observed red shift of the 517-nm peak may be understood in terms of the model by Bandeira *et al.*[10] The observed (3—4)-nm red shifts of the high-energy peak with decreasing light modulation frequency in the PA spectra of Fig. 8(a) render further credibility to the argument concerning the intraband excitation origin of the red-shifted shoulder in Fig. 10(a). The PC magnitude spectral similarity under both chopped and unmodulated optical excitation can be understood from the fact that the PC response is independent of the photoacoustic thermal diffusion length which is ultimately the reason for the frequency dependence of Eq. (2). Therefore, no frequency dependence of the PC signal is expected and no red shift of the intrinsic shoulder at $\omega_{ac} \rightarrow 0$, in agreement with Figs. 5(a) and 10(a). Furthermore, the spectral features of the PC response in the presence of a dc electric field under unmodulated illumination were entirely similar to those of Figs. 5(a) and 10(a).

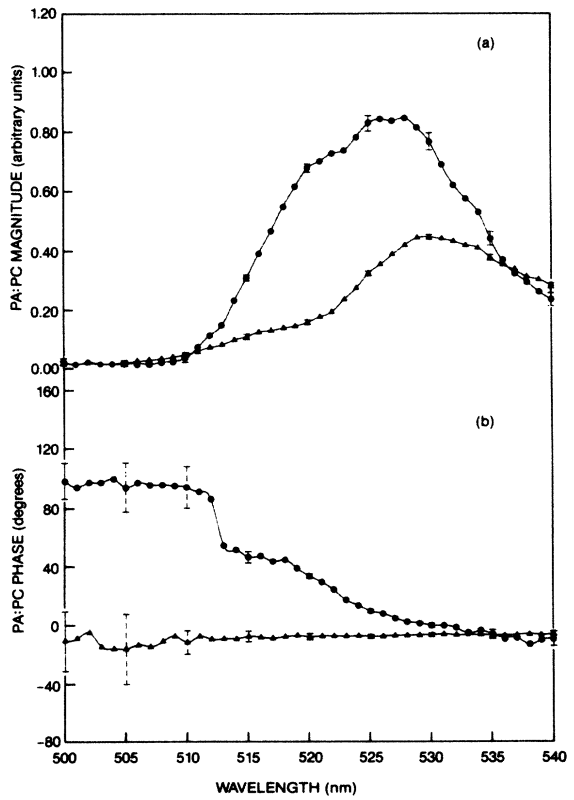

FIG. 10. (a) Magnitude spectra of PA (—●—●—) and PC (—▲—▲—) responses with an ac transverse electric field of 20 V peak-to-peak. Field modulation frequency: 20 Hz; spectral resolution: 2 nm (b) Phase spectra of PA (—●—●—), and PC (—▲—▲—) responses.

Under unmodulated excitation and ac photocarrier orientation, the generation and recombination of free carriers are dc phenomena, which implies that the carrier lifetimes do not affect the PA phase response.[35] The increase in the PA phase lag observed in Fig. 10(b) is, thus, solely due to the finite diffusion time of the receding Joule effect-induced heat centroid in the crystal from the near surface to the bulk with increasing wavelength. The PC phase spectrum is independent of the photogenerated carrier density, which is temporally constant and varies with photon energy. It depends, however, on the carrier diffusion length[44]

$$L(\omega_{ac}) = \frac{L_n}{(1+i\omega_{ac}\tau)^{1/2}} \tag{4}$$

and, therefore, in the limit $\omega_{ac} \rightarrow 0$, it is independent of the photocarrier lifetime τ. The PC phase is thus expected to be independent of the mechanism producing the photocurrent at $\omega_{ac}=0$. It depends solely on the speed of photocarrier response to the ac electric field, which is essentially infinite at the modulation frequencies of our experiments. As a result of the above considerations, a spectrally flat PC phase response at zero lag would be expected, in agreement with Fig. 10(b).

We have also studied the effect of the field modulation frequency on the PA and PC spectral responses shown in

Fig. 11. Part (a) of this figure shows that, with increasing ω_{ac}, the magnitude of the 523-nm PA shoulder becomes spectrally resolved and fractionally increases in relation to the frequency independent 529-nm maximum. The latter remains at 529 ± 0.5 nm at all frequencies, while the former exhibits a blue shift of about 3 nm behaving in a manner analogous to the one observed in Fig. 8(a). The PC magnitude response, Fig. 11(b) exhibits a very weak dependence on ω_{ac} with no clear trends. This is expected, since the free carrier density within the crystal, which is directly related to the PC magnitude, is not affected by the low modulation frequency, of the ac electric field relative to the carrier response rate.

PA magnitude versus electric field modulation frequency f_{ac} curves were plotted for the 522- and 529-nm peaks of Fig. 11(a). The frequency dependences were found to be $f_{ac}^{1.2\pm0.2}$ at 522 nm and $f_{ac}^{1.65\pm0.2}$ at 529 nm. The latter peak was previously shown to be in the optically transparent, thermally thick limit of the RG theory. The former peak, with an associated[7] optical-absorption coefficient $\beta(522\text{ nm})=10\text{ cm}^{-1}$, is close to photoacoustic saturation and, therefore, essentially opaque. For finite optical modulation frequencies ($f\neq0$), the RG theory predicts an $f^{-0.5}$ dependence due to the phase lag of the amount of thermal energy generated in the crystal upon absorption of the radiation, plus additional contributions to the f dependence, determined by the optical and thermal properties of the material.[41] In this experimental mode, the $f^{-0.5}$ dependence will be eliminated under unmodulated optical absorption and subsequent heat generation ($f=0$), while the material-related thermal contributions to the f_{ac} dependence will be present. It is, therefore, expected that a general f_{ac}^{-2} dependence will prevail in the optically transparent region, with a $f^{-1.5}$ ac dependence in the opaque region. The values for the measured f_{ac} dependences of the 529- and 522-nm peaks are in rough agreement with the qualitatively generated power dependences given above, in view of the crude argument used to justify these dependences.

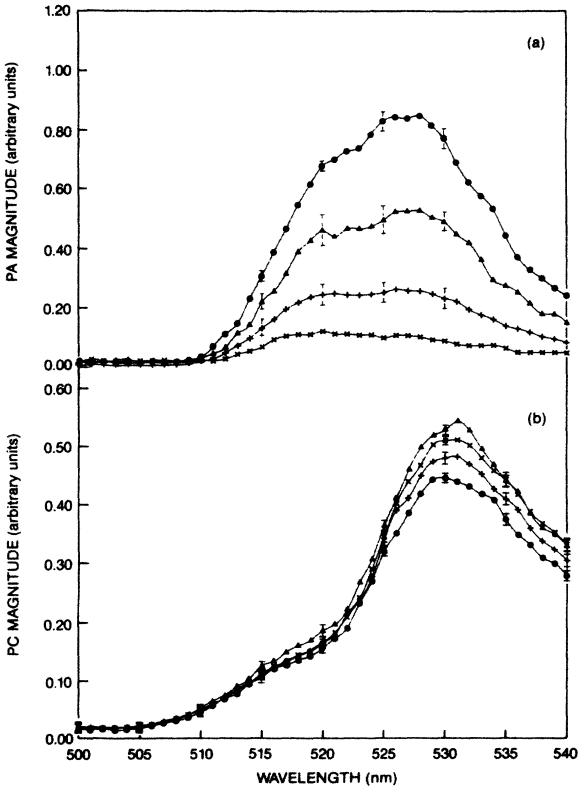

FIG. 11. (a) PA and (b) PC magnitude spectra of CdS with a 20 V peak-to-peak AC applied electric field, 2-nm spectral resolution, and unmodulated optical excitation. Electric field modulation frequency: 20 Hz (—●—●—); 35 Hz (—▲—▲—); 50 Hz (— + — + —); and 100 Hz (—x—x—).

D. Secondary PA and PC spectra: modulated optical excitation with a dc electric field

CdS and other photoconductors (ZnS, ZnSe, CdSe, ZnTe) are known to exhibit photoconductivity sensitization in the visible, and quenching in the infrared (ir) spectral region with maxima at photon energies of, or lower than, 1.65 eV (CdS) (Ref. 4), i.e., at around 750 nm and beyond with the onset of ir quenching commencing at about 560 nm for CdS at room temperature.[4] To investigate the effects of such phenomena on the PA and PC responses of CdS, secondary spectra were recorded as shown in Fig. 12. Photoacoustic and photoconductive sensitization is observed for $\lambda\leq526$ nm and a response magnitude reversal for $\lambda>526$ nm. Wada *et al.*[11] have recently extended the ir quenching spectral region to the visible, by reporting PA, PC, and PL spectral quenching of a low-resistivity n-type CdS undoped single crystal at wavelengths below 750 nm, down to about 400 nm. The behavior of the secondary spectra of Figs. 12(a) and 12(b), more complex than that of Ref. 11, is in agreement, however, with a hypothesis concerning the nature of band-gap-active defects in CdS, which has been advanced by Rose.[45] According to this hypothesis, two generic classes of defects, acting as recombination centers, are predominant throughout the band gap. Class I defects have a small-capture cross section for holes and a large-capture cross section for electrons, once they have captured a hole,

$$[V_s^-]^+ + h^+ \rightarrow [V_s]^{2+}\ ,$$
$$[V_s{}^{2-}]^0 + h^+ \rightarrow [V_s^-]^+\ . \tag{5}$$

V_s represents an anion (here assumed to be sulphur) vacancy, with the sign inside the bracket representing the number of trapped electrons, and the sign outside the bracket indicating the effective charge of the defect with respect to the rest of the crystal. Class II defects have a large-capture cross section for holes and are filled with electrons in the dark. These defects lie close to the valence band edge and they capture holes according to

$$[V_{Cd}]^{2-} + h^+ \rightarrow [V_{Cd}{}^+]^-\ ,$$
$$[V_{Cd}^+]^- + h^+ \rightarrow [V_{Cd}]^+\ , \tag{6}$$

where V_{Cd} represents a cation (here assumed cadmium) vacancy in the pure crystal. According to Rose's hypothesis, then, in the proper spectral range ($\lambda\leq526$ nm in

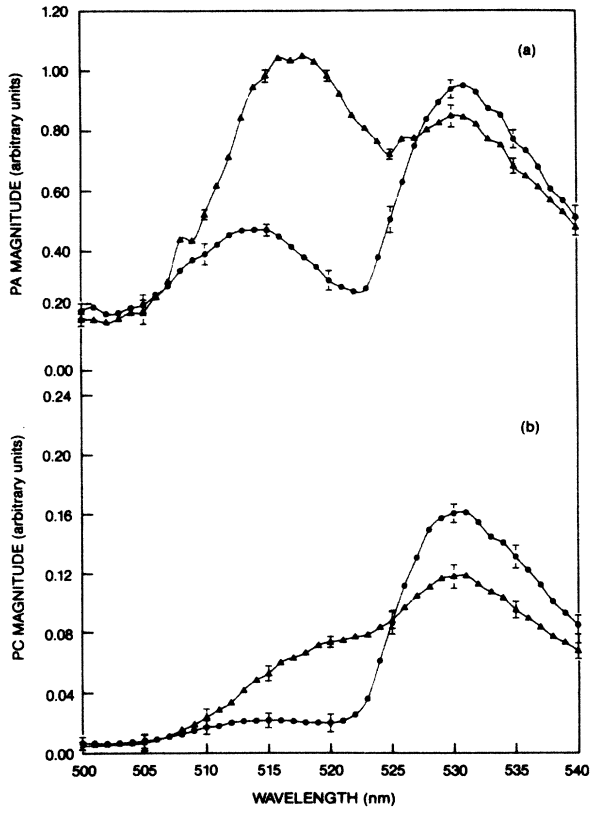

FIG. 12. Secondary spectra of CdS with a 20-V DC applied electric field and 2-nm spectral resolution. Light modulation frequency: 20 Hz. (a) PA spectrum. No primary light source (—●—●—); with primary light source (—▲—▲—) (b) PC spectrum. No primary light source (—●—●); with primary light source (—▲—▲—).

Fig. 12), holes formed by the primary excitation will concentrate in the class II centers via Eq. (6), while electrons, which occupied these centers in the dark, will be transferred via the conduction and valence bands to the energetically higher lying class I centers, due to the large electronic capture cross section of these centers. These defects will thus be eliminated as efficient recombination centers due to their occupancy by the transferred electrons, with a resulting increase in the lifetime of free electrons and, therefore, an increase in the photoconductivity of the crystal. A simultaneous increase in the PA signal will ensue as the amount of nonradiative recombination will be proportional to the total (increased) number density of free electrons. This defect structure can also be used to explain the quenching observed in Fig. 12 for $\lambda > 526$ nm. This phenomenon will occur only when class II defects are acting as recombination centers, i.e., when electrons are excited from the valence band to class II centers in the proper spectral range ($\lambda > 526$ nm), thus freeing holes which will eventually be transferred to class I defects and turn these defects into efficient traps for electronic capture. Bube[4] has given the requirements imposed on electron and hole Fermi-level positions for such excitations to occur, and has identified the spectral positions of three class II energy levels in the CdS band gap, associated with infrared quenching. Both the PC and PA secondary signals are expected to decrease with quenching with respect to the dark (primary zero) level, as the number density of free electrons will decrease in the presence of the class I centers of Eq. (5). Both our data, Fig. 12, and those of Wada *et al.*[11] indicate that quenching in pure *n*-type CdS crystals can also occur under primary irradia-

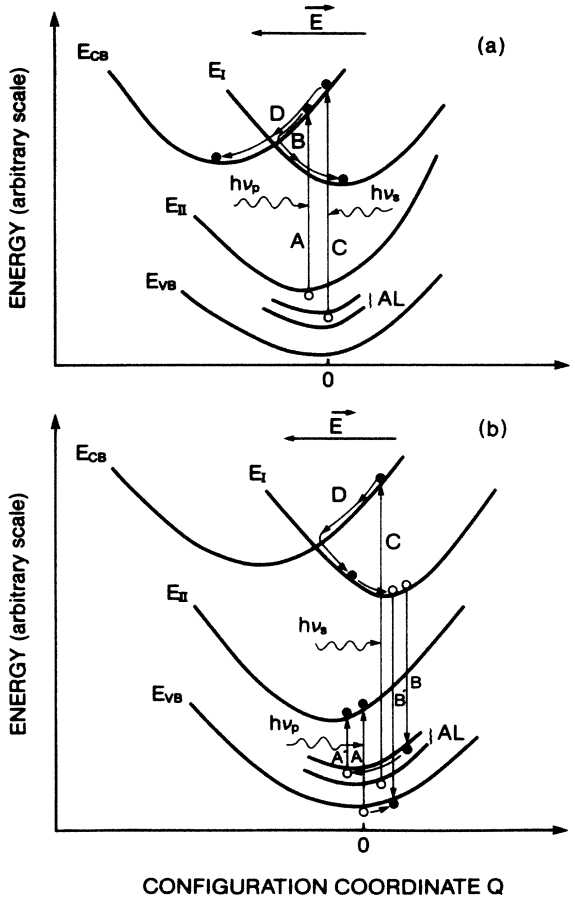

FIG. 13. (a) Franck-Condon configuration coordinate diagram of possible sensitization mechanism in high-resistivity pure *n*-type CdS. Process A: primary optical excitation of electron from class II defect state to excited state in the conduction band. Process B: intraband deexcitation and cross-over to class I defect state. Process C: secondary excitation from low-lying acceptor level(s) (AL) to excited state in the conduction band. Process D: intraband deexcitation to the bottom of the conduction band with no crossover to occupied class I states, resulting in free-electron density increase (sensitization); ν_p and ν_s are primary and secondary optical excitation frequencies, respectively. $\nu_s \rightarrow \lambda_s \leq 526$ nm; (●) electron; (○) hole. (b) Franck-Condon configuration diagram of possible quenching mechanism in high-resistivity pure *n*-type CdS. Process A,A′: primary optical excitation of electron from the valence band or low-lying acceptor level(s) (AL) to class II defect state. Process B,B′: hole transfer from AL or VB to class I defect state. Process C: secondary excitation from low lying AL to excited state in the conduction band. Process D: intraband deexcitation and cross-over to unoccupied class I defect state resulting in free-electron density decrease, through trapping (quenching); $\nu_s \rightarrow \lambda_s > 526$ nm.

tion in the red spectral region ($\lambda < 600$ nm), followed in our high-resistivity sample by a sensitized spectral region with a threshold wavelength at about $\lambda_t \approx 526$ nm. Figure 13 is a configuration coordinate diagram indicating a possible transition mechanism leading to a qualitative explanation of the secondary PA and PC sensitized and quenched spectral responses of Fig. 12, based on Rose's hypothesis. The expected effects of the applied electric field in Fig. 13 are primarily (i) an enhancement of the velocity distribution of free carriers, with a mean velocity increase and the resulting lowering of the capture rate at the shallow class I defect centers;[46] and (ii) the Poole-Frenkel effect, due to which the ionization energy along the field direction **E** is reduced.[47] Electric field effects for deep levels such as class II defect centers are expected to involve multiphonon mechanisms.[48]

IV. CONCLUSIONS

The present work has established the nonequivalence between transmission and photoacoustic spectra of CdS, especially in the sub-band-gap region where lattice defects and wavelength-dependent nonradiative processes are expected to contribute a wealth of information to the PA spectrum unparalleled by transmission spectroscopic information. Two resolved PA peaks between 515 and 530 nm appeared under 2-nm spectral resolution, with either a dc or ac electric field applied, and were assigned to (i) intrinsic band-to-band electronic transitions (high-energy peak), thus conclusively verifying experimentally the theory by Bandeira *et al.*[10] for the first time, as far as its applicability in the super-band-gap region is concerned; and (ii) an increased nonradiative quantum efficiency in the sub-band-gap region (low-energy peak), which is also quantitatively in agreement with the theoretical model presented in Paper II. These assignations were further supported experimentally by the modulation frequency responses of the peaks and by comparisons with PC spectra. The latter spectra were shown to be unable to resolve spectrally the two peaks and thus PAS is found to have the advantage of spectral resolution over PCS, with modulation frequency controlling peak separation. Both PA and PC secondary spectra exhibited sensitization in the spectral range of the high-energy peak and quenching in the spectral range of the low-energy peak. These phenomena were qualitatively interpretable in terms of Rose's hypothesis[45] involving the capture role of defect centers in the band gap of CdS. The deduction of the above conclusions concerning the interpretations of the PA spectral features observed in CdS was enhanced through consistency arguments by the simultaneous use of the PC spectroscopic probe, however, such deduction would have *not been possible* with the use of PCS only, due to the poor peak resolution of the latter technique.

ACKNOWLEDGMENTS

The authors wish to acknowledge the financial support of the Natural Sciences and Engineering Research Council (NSERC) of Canada throughout the work accomplished in both parts of this report.

[1]C. C. Klick, Phys. Rev. **89**, 274 (1953).
[2]D. Dutton, Phys. Rev. **112**, 785 (1958).
[3]D. G. Thomas, J. J. Hopfield, and M. Power, Phys. Rev. **119**, 570 (1960).
[4]R. H. Bube, Phys. Rev. **99**, 1105 (1955).
[5]R. H. Bube, J. Phys. Chem. Solids **1**, 234 (1957).
[6]I. Uchida, J. Phys. Soc. Jpn. **22**, 770 (1967).
[7]R. H. Bube, and L. A. Barton, RCA Rev. **111**, 564 (1959).
[8]K. Yamamoto, Y. Yamazoe, S. Kameyama, and K. Abe, Appl. Phys. Lett. **29**, 671 (1976).
[9]K. Wasa, K. Tsubouchi, and N. Mikoshiba, Jpn. J. Appl. Phys. **19**, L475 (1980).
[10]I. N. Bandeira, H. Closs, and C. C. Ghizoni, J. Photoacoust. **1**, 275 (1982).
[11]H. Wada, H. Yoshioka, J. Morimoto, and T. Miyakawa, Jpn. J. Appl. Phys. **24**, Suppl. 24-1, 217 (1985).
[12]T. Hata, T. Hatsuda, M. Kawakami, and Y. Sato, Jpn. J. Appl. Phys. **24**, Suppl. 24-1, 204 (1985).
[13]T. Hata, Y. Sato, Y. Nagai and T. Hada, Jpn. J. Appl. Phys. **23**, Suppl. 23-1, 75 (1984).
[14]R. Nitsche, J. Phys. Chem. Solids **17**, 163 (1960).
[15]J. Powderly, Eagle-Pitcher, Inc. (Miami, Oklahoma) (private communication).
[16]J. R. Cutter and J. Woods, J. Crystal Growth **47**, 405 (1979).
[17]J. L. Boone and G. Cantwell, J. Appl. Phys. **57**, 1171 (1985).
[18]R. W. Smith, Phys. Rev. **97**, 1525 (1955).
[19]F. A. Kröger, G. Diemer, and H. A. Klasens, Phys. Rev. **103**, 279 (1956).
[20]S. P. Gaplevskaya, L. S. Zavertannaya, A. L. Rvachev, and E. I. Tishchenko, Fiz. Tekh. Poluprovodn. **6**, 385 (1972) [Soviet Phys.—Semiconductors **6**, 327 (1972)].
[21]P. Rochon and T. J. Racey, J. Photoacoust. **1**, 475 (1984).
[22]A. Rosencwaig, Anal. Chem. **47**, 592A (1975).
[23]A. J. Bard, Analusis **6**, 277 (1978).
[24]D. M. Munroe and H. S. Reichard, Am. Lab. **9**, 199 (1977).
[25]R. Takaue, M. Matsunaga, and K. Hosokawa, J. Appl. Phys. **56**, 1543 (1984).
[26]T. Hata, Y. Sato, and M. Kurebayashi, Jpn. J. Appl. Phys. **22**, Suppl. 22-3, 205 (1982).
[27]H. D. Bruer, Naturwissenschaften **67**, 91 (1980).
[28]H. Gobrecht, Z. Physik **136**, 224 (1953).
[29]R. H. Bube, Phys. Rev. **98**, 431 (1955).
[30]M. Cawdona and G. Harbeke, Phys. Rev. A **137**, 1467 (1965).
[31]D. G. Thomas and J. J. Hopfield, Phys. Rev. **116**, 573 (1959).
[32]R. A. Smith, *Semiconductors,* (Cambridge University Press, 1959), Chap. 3.
[33]J. Lambe, Phys. Rev. **98**, 985 (1955).
[34]I. M. MacKintosh and J. W. Allen, Proc. Phys. Soc. London Sect. B, **68**, 985 (1955).
[35]A. Mandelis, Y. C. Teng, and B. S. H. Royce, J. Appl. Phys. **50**, 7138 (1979).
[36]L. D. Merkle and R. C. Powell, Chem. Phys. Lett. **46**, 303 (1977).
[37]R. H. Bube, J. Chem. Phys. **23**, 18 (1955).
[38]R. H. Bube, *Photoconductivity of Solids* (Wiley, New York, 1960), p. 391.

[39]Y. S. Park and D. C. Reynolds, Phys. Rev. **132**, 2450 (1963).
[40]J. J. Hopfield, J. Phys. Chem. Solids **15**, 97 (1960).
[41]A. Rosencwaig and A. Gersho, J. Appl. Phys. **47**, 64 (1976).
[42]C. L. Cesar, H. Vargas, J. Mendes Filha, and L. C. M. Miranda, Appl. Phys. Lett. **43**, 556 (1983).
[43]J. P. Roger, D. Fournier, A. C. Boccara, R. Noufi, and D. Cahen, Thin Solid Films **128**, 11 (1985).
[44]J. P. McKelvey, *Solid State and Semiconductor Physics* (Harper & Row, New York, 1966), Sect. 13.6.
[45]A. Rose, Phys. Rev. **97**, 322 (1955).
[46]V. L. Bonch-Bruevich and E. G. Landsberg, Phys. Status Solidi **29**, 9 (1968).
[47]A. M. Stoneham, *Theory of Defects in Solids* (Clarendon, Oxford, 1975), Chap. 12.
[48]E. N. Koral, Fiz. Tverd. Tela (Leningrad) **19**, 2266 (1977) [Sov. Phys.—Solid State **19**, 1327 (1977)].